Journal of Magnetism and Magnetic Materials 630 (2025) 173311

Contents lists available at ScienceDirect

Journal of Magnetism and Magnetic Materials

journal homepage: www.elsevier.com/locate/jmmm

# Multi-scale magnetic aging model: Precipitation kinetics and magnetic hysteresis coupling

Fabien Dancoisne [a,b], Hugo Helbling [c], Abdelkader Benabou [b], Stéphane Clénet [b], Myriam Dumont [a,*]

[a] Arts & Métiers Institute of Technology. (MSMP-EA7350) Mechanics, Surfaces and Materials Processing, 8 bd Louis XIV, Lille Cedex, 59046, France
[b] Univ. Lille, Arts & Métiers Institute of Technology, Centrale Lille, HEI. (L2EP-EA2697) Laboratoire d'Électrotechnique et d'Électronique de Puissance, Bâtiment ESPRIT, Avenue Henri Poincaré, Villeneuve d'Ascq, 59655, France
[c] Université Claude Bernard Lyon 1, Ampère, UMR5005, INSA Lyon, École Centrale de Lyon, CNRS, Villeurbanne, F-69100, France

ARTICLE INFO

*Keywords:*
Coercive field
Hysteresis losses
Jiles–Atherton (J-A)
Johnson–Mehl–Avrami–Kolmogorov (JMAK)
Magnetic aging
Non-oriented electrical steels (NOES)
Precipitation kinetics

ABSTRACT

Operating temperatures of electrical machines are known to cause various effects on magnetic performances and losses. On the one hand, reversible contributions may reduce iron losses through temporary lowering of conductivity, which in turn reduces eddy-current losses. On the other hand, when specific thermal conditions are met, the time–temperature combination may lead to irreversible changes of the magnetic material properties. This latter phenomenon, the so-called magnetic aging, needs to be addressed to further improve energy efficiency, predict and reduce heat-dissipated iron losses. These service conditions indeed lead to changes in the microstructure of the electrical steels. Thus, iron losses suffer from these structural modifications as well as long exposure to constant operating temperatures; magnetic aging results from carbides precipitation and impacts the magnetization of these steels. The present paper hence explores a multi-scale approach, coupling the Johnson–Mehl–Avrami–Kolmogorov (JMAK) precipitation kinetics with a static Jiles–Atherton (J-A) model of magnetic hysteresis for a non-oriented soft ferromagnetic Fe-Si steel. Based on an experimental analysis for temperatures ranging from 180 °C to 200 °C, the applicability of the chosen approaches will be explored and a parameter-based modeling of magnetic aging will be proposed and proved to be in good agreement with measurement data.

## 1. Introduction

Tackling with global warming effects, from an industrial standpoint, often implies drastic improvements and a necessary harnessing of energy efficiency, especially with energy sources and conversion systems such as rotating electrical machines. In these applications, performance management is as preponderant as losses reduction, above all in the choice and design of the soft ferromagnetic alloys used to built them. These materials are subject to losses of electromagnetic origin, among them the so-called iron losses playing a most impacting role. However, such steels may suffer from an irreversible degradation of magnetic properties caused by long exposure to medium operating temperatures; the present article focuses on the 160–200 °C range. This phenomenon, known as magnetic aging, leads to increased heat dissipation losses and reduced efficiency. Investigating magnetic aging sources in non-oriented iron-silicon steel sheets (NOES), widely used in energy conversion systems, begins with the very chemical composition of the materials at play. Indeed, for a given Fe–Si alloy (with up to 3 wt% Si), other elements are still present, mainly due to elaboration, manufacturing and forming processes: carbon (C), nitrogen (N), phosphorus (P)... Although in rather small quantities (several tens to several hundreds of ppm), their effects remain significant. Among those, the carbon content plays a major role in magnetic aging kinetics through its ability to precipitate into carbides, in particular cementite ($Fe_3C$), that hinders magnetization. In the literature, numerous papers have treated this phenomenon decades over, starting with the effects second-phase particles have on coercive field [1,2], *i.e.*, the magnetic field intensity that must be applied to a saturated material to cancel out its magnetization. While the volume fraction of said particles directly causes an increase of the coercive field [3–5], other parameters, such as their size, their number as well as their chemical composition seem to also correlate to magnetic aging, as they all tend to curb magnetic domains enlargement during magnetization through domain wall movements impingement, *i.e.*, creating pinning sites leading to greater energy dissipation during wall displacements. Hence, from [3,5,6], it is clear

* Corresponding author.
*E-mail address:* myriam.dumont@ensam.eu (M. Dumont).

https://doi.org/10.1016/j.jmmm.2025.173311
Received 4 December 2024; Received in revised form 18 June 2025; Accepted 18 June 2025
Available online 16 July 2025

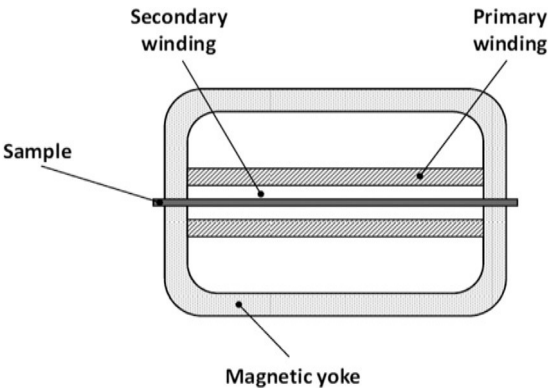


**Fig. 1.** Single Sheet Tester measurement device.

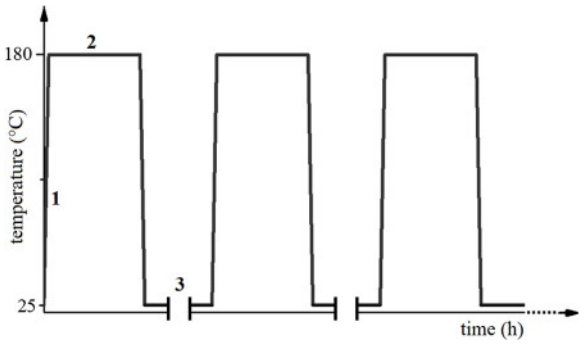


**Fig. 2.** Followed experimental protocol. (1) Heating, (2) Aging treatment, (3) Cooling to room temperature and SST characterization.

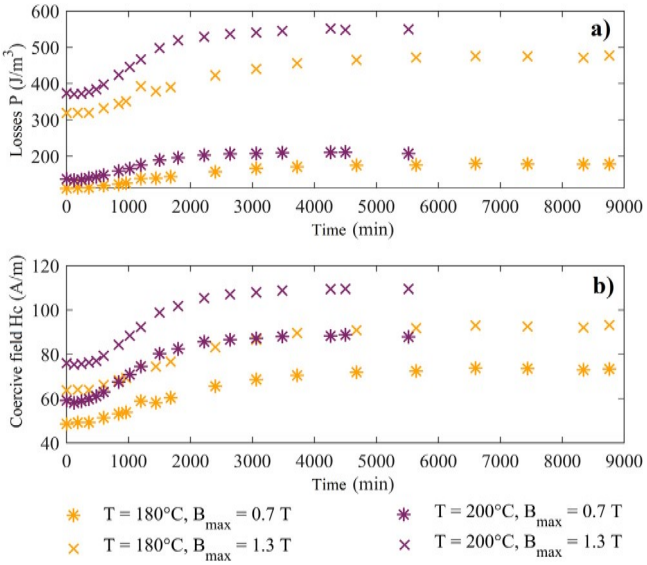


**Fig. 3.** (a) Measured hysteresis losses and (b) measured coercive field evolution with time at 5 Hz of M600-65A samples aged at 180 °C and 200 °C, for different induction levels at $f = 5$ Hz.

that the more carbon there is, the more precipitates can be formed, the higher the toll on magnetization and thus on performances. Plus, it also highlights that higher in-service temperatures are responsible for an acceleration of the aging kinetics [7], while longer aging periods result in a heightened amount of maximal losses that may however plateau or even slightly drop once all the C has precipitated. Furthermore, links have been established between precipitation kinetics and magnetic losses [5,8], with initial carbon content being a driving condition for aging intensity. On a more recent note, the effects of isothermal aging on automotive bulk pieces [9] and on low-carbon NOES [10] have been investigated in an attempt to model iron losses and coercive field variation with the classical Johnson–Mehl–Avrami–Kolmogorov (JMAK) precipitation approach, paired with Arrhenius' expression to highlight temperature effects. While those latter propositions provide a simple yet quite accurate method to the modeling of losses when coupled with the Steinmetz' equation of losses for example [9], further developing a program that considers the time-evolution of magnetic quantities accounting for hysteresis, could be beneficial. Therefore, the present article will explore a method to extract hysteresis parameters from measurement data to then build a coupling with another model to describe carbide precipitation. First, it will expand on the experimental protocol carried out as well as its results, so that data can be analyzed. The next section will focus on explaining precipitation kinetics, the modeling with the JMAK approach and the presentation of the Jiles–Atherton (J–A) model of magnetic hysteresis. Relationships between quantities will be detailed in order to validate the choice of models and, eventually, a first attempt at coupling both these models, through the pinning coefficient $k$, will be presented and its multi-scale results discussed.

## 2. Experimental methodology

The main objectives of this experimental analysis are to acquire comprehensive magnetic aging data and to highlight relationships between quantities of interest that will lateron justify the use of the JMAK precipitation model.

### 2.1. Experimental protocol

An experimental analysis has been conducted on two fully processed, cold-rolled, non-oriented Fe-2.3 wt%Si M600-65A $300 \times 20 \times 0.65$ mm samples aged at 180 °C and 200 °C for a total of 92 h and 146 h, respectively, as per described in [10]. Each sample is first characterized on a Single Sheet Tester device (SST, see Fig. 1) at room temperature, at the frequency of $f = 5$ Hz (quasi-static case). Then, they undergo an isothermal treatment inside an oven while being periodically taken out for magnetic characterization at room temperature, until the total aging time is elapsed. Fig. 2 summarizes the followed experimental protocol. Each measurement time-step provides material data under sinusoidal magnetic flux density input of $B_{max} \in [0.1; 1.6]$ T as well as magnetic properties evolution.

### 2.2. Experimental results

Fig. 3.a illustrates the quasi-static hysteresis losses $P$ (J/m$^3$) evolution with aging time, at 180 °C and 200 °C and for two different magnetic induction magnitudes, namely 0.7 and 1.3 T, while Fig. 3.b, on the other hand, focuses on the coercive field $H_c$ (A/m) evolution with time, considering the same aging temperatures and induction levels.

Looking at Fig. 3, it clearly appears that magnetic aging increase both $P$ and $H_c$ during the first dozens of hours before plateauing when its maximal effect is reached. To further emphasize this phenomenon, Fig. 4 shows experimental hysteresis loops before and after 92 h of aging at 200 °C. Whether hysteresis losses or coercive field are considered, the higher the temperature, the faster the aging kinetics, as stated in [6]. The evolution over time of the curves seems to echo previous analyses [9], displaying the same aging-induced increase in both losses and coercive field before reaching a plateau value where most of the carbon has been converted into precipitates.

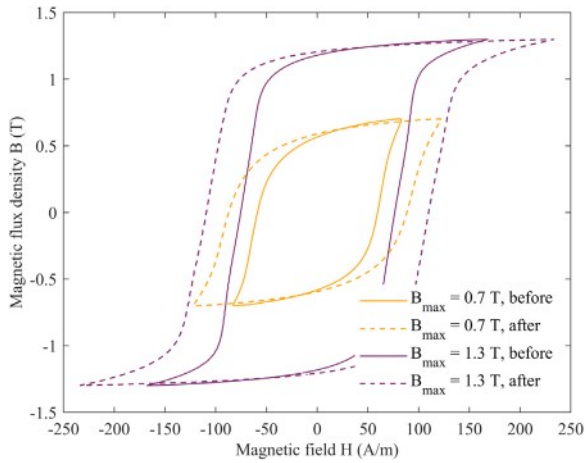


**Fig. 4.** Measured hysteresis loops before and after 92 h of aging at 200 °C, 5 Hz.

## 3. Modeling methodology

### 3.1. Precipitation kinetics model

Looking back at earlier analyses on magnetism and magnetic materials, relationships between inclusion volume fraction and coercive force increase have been established [1,2]. The coercive field is usually related to the amount of magnetic field required to demagnetize one material and governs the width of the hysteresis loop. Hence, since the loop area is proportional to the hysteresis losses, the higher the coercivity value, the wider the loop, the greater the losses. To obtain a coupling between precipitation kinetics and these quasi-static losses, a simple model describing precipitation will be derived in the following so that relationships between quantities can be established to be later linked to a phenomenological magnetic hysteresis approach. According to the classical theory of phase transformations, carbide formation follows three successive phases: nucleation, growth and coarsening [11,12], the latter not being accounted for in the following. Over time, if the operating temperature is maintained, a driving force coupled with diffusion causes movements and gathering of C atoms in nuclei; hence the name nucleation. These particles progressively enlarge up to consuming the supersaturated C in the iron matrix; here only cementite ($Fe_3C$) will be considered for the sake of simplicity. From then on, the use of the JMAK approach [13–16] expresses a simplified phase transformation rate $Y$ built upon nucleation and growth kinetics:

$$Y(t) = \frac{v_{Fe_3C}(t) - v_{min}}{v_{max} - v_{min}} = \frac{v_{Fe_3C}(t)}{v_{max}}, \tag{1}$$

with $v_{Fe_3C}(t)$ the time-dependent precipitate volume fraction (-), $v_{max} = 0$ its initial amount and $v_{max}$ its maximal value, generally equal to the equilibrium volume fraction at the considered temperature. This expression can be further rewritten with coefficients summarizing phase transformation mechanisms, as (2) suggests:

$$Y(t) = 1 - \exp\left(-\mathcal{K}_T t^n\right), \tag{2}$$

where $n$ is the Avrami index ($n = 4$ for spherical nuclei) and $\mathcal{K}_T$ regroups nucleation and growth stages into a single identifiable value. To identify the parameters used in (2), linear regression technique (3) is applied and, as the literature suggests [17], $n$ is found to be constant and temperature-independent, which reduces the number of actual aging-related parameters.

$$\ln(-\ln(1 - Y)) = \ln(\mathcal{K}_T) + n\ln(t). \tag{3}$$

Furthermore, $\mathcal{K}_T$ in (2) can be replaced by its Arrhenius equivalent (4), to account for different operating temperatures or complex heating cycles.

$$\mathcal{K}_T = -k_0 \exp\left(-\frac{Q}{\mathcal{R}T}\right), \tag{4}$$

with $k_0$ a velocity constant ($s^{-n}$), $Q$ the activation energy for the phase transformation (J/mol), $T$ the temperature (K) and $\mathcal{R} = 8.314$ (J/K/mol) the universal gas constant. As a result, instead of having multiple $\mathcal{K}_T$ for different test temperatures, only a $[Q, k_0]$ couple is required for a given temperature range.

**Table 1**
Jiles–Atherton parameters.

| Parameter | Meaning | Unit |
|---|---|---|
| $\alpha$ | Inter-domain coupling | – |
| $a$ | Anhysteretic form factor | A/m |
| $c$ | Domain wall bending coefficient | – |
| $k$ | Pinning factor (hysteresis) | A/m |
| $M_{sat}$ | Saturation magnetization | A/m |

### 3.2. Magnetic hysteresis model

Now that precipitation kinetics have been derived by means of the JMAK approach, this section presents the Jiles–Atherton (J–A) model of static magnetic hysteresis and aims at proving that one of its parameters actually follows a JMAK-styled law and therefore translate magnetic aging. The static J–A model [18,19] proposes a parameter-based fitting of hysteresis (or B–H) loops. Based upon a phenomenological energy balance involving reversible and irreversible contributions to magnetization, its expression of the effective magnetic field $H_e$(5) recalls up the molecular field theory [20] — which incidentally applies to atomic ferromagnetism — to express the coupling between magnetic domains:

$$H_e = H + \alpha M, \tag{5}$$

where $M$ is the total magnetization $M$ (A/m) of a material and $\alpha$ a coupling factor between domains (see Table 1). While the reversible part $M_{rev}$ of magnetization features domain walls slowly bending around defects then coming back to their initial position if the magnetic field decreases at low-amplitude, the irreversible pinning site jump-over $M_{irr}$, possible when $H$ increases further (6), dissipates more energy and increases coercive field until saturation is reached.

$$M = c(M_{an} - M_{irr}) + M_{irr} \tag{6}$$

The model then resolves the following Eqs. (7)–(9), while the material-specific parameter meanings are summarized in Table 1. In (8), the parameter $\delta = \pm 1$ according to the evolution of the field on the ascending (+1) or descending (−1) hysteresis branch.

$$M_{an} = M_{sat}\left(\coth\left(\frac{H + \alpha M}{a}\right) - \left(\frac{a}{H + \alpha M}\right)\right), \tag{7}$$

$$\frac{dM_{irr}}{dH_e} = \frac{M_{an} - M_{irr}}{k\delta}, \tag{8}$$

$$\frac{dM}{dH} = \frac{(1-c)\frac{dM_{irr}}{dH_e} + c\frac{dM_{an}}{dH_e}}{1 - \alpha c\frac{dM_{an}}{dH_e} - \alpha(1-c)\frac{dM_{irr}}{dH_e}}, \tag{9}$$

where $M_{an}$ is the anhysteretic magnetization and $M_{sat}$ the saturation, both in A/m.

From the literature-based definitions above, the pinning factor $k$ seems to be directly related to the amount of hindrance domain walls endure, hence interacting with the material coercivity and losses. It is therefore relevant to treat its time-dependent evolution as a proof of magnetic aging. As per developed in the literature [21–23], hysteresis model parameters are obtained by fitting several experimental loops measured on an SST device for a quasi-static $f = 5$ Hz case. First, initial, anhysteretic and coercive susceptibilities $\chi_0$, $\chi_{an}$, $\chi_c$, respectively, are measured on a major loop at a given aging temperature $T_{age}$ and at

$t_{age} = 0$ min, then used to compute a first coarse set of parameters in (10) and (11).

$$a = \frac{M_{sat}}{a}\left(\frac{1}{\chi_{an}} + \alpha\right) \quad c = \frac{3a\chi_0}{M_{sat}} \tag{10}$$

$$k = \frac{M_{an}(H_c)}{1-c}\left(\alpha + \frac{1}{\frac{\chi_c}{1-c} - \left(\frac{c}{1-c}\right)\left(\frac{dM_{an}(H_c)}{dH}\right)}\right) \tag{11}$$

These parameters then serve as the starting point of a constrained optimization procedure which aims at minimizing the difference between each value of an experimental $B_{EXP,i}$ ascending hysteresis branch and its simulated $B_{SIM,i}$ counterpart:

$$F_{obj} = \sum_{i=1}^{N}\left(B_{EXP,i} - B_{SIM,i}\right)^2, \tag{12}$$

subject to the non-linear equality constraint (13) proposed by [22]:

$$C_{in} = \frac{\mathcal{A}_{SIM} - \mathcal{A}_{EXP}}{\mathcal{A}_{EXP}} \times 100 - \epsilon, \tag{13}$$

where $\mathcal{A}_{SIM}$ and $\mathcal{A}_{EXP}$ are the simulated and experimental loop areas in J/m$^3$ respectively, as expressed by (14), and $\epsilon$ an arbitrarily-chosen threshold percentage limiting the error deviation.

$$\mathcal{A}_i = \int_{-b}^{b} H_i dB_i \tag{14}$$

## 4. Results

### 4.1. JMAK approach applied to magnetic properties

As demonstrated in [9], the goal of this section lies in the description of losses and coercive field evolution with time by means of the aforementioned JMAK approach. From [1], it is possible to consider a linear relationship between precipitate volume fraction and coercive field increase. Thus, the JMAK model may express coercivity evolution through its transformation rate (15):

$$Y(t) = \frac{H_c(t) - H_{c,min}}{H_{c,max} - H_{c,min}} \tag{15}$$

Since Fig. 5 highlights a linear dependency between magnetic losses and measured coercive field, this ensures the use of a transformation rate through the JMAK model. Consequently, (2) can be adapted to either losses or coercive field, as (16) shows:

$$Y(t) = \frac{P(t) - P_{min}}{P_{max} - P_{min}} \tag{16}$$

In theory, $Y$ should not depend on magnetic flux density for it only relies on microstructural characteristics and solely represents the rate at which quantities evolve but not their magnitude; in fact, as the transformation rates of coercive field and losses are drawn on Fig. 6, it is possible to consider, at the very least for the samples used in this study and at the working induction levels [24], that transformation rates do not depend on magnetic induction, as the superimposed curves suggest. From then on, the general Eq. (2), whose coefficients are identified in each case, is used to draw coercive field evolution with time on Fig. 7.a and its hysteresis losses counterpart on Fig. 7.b, with the same set of parameters.

### 4.2. JMAK approach applied to J–A pinning factor evolution

Fig. 8 summarizes the whole method: firstly, several experimental hysteresis loops and their susceptibilities serve as inputs. As mentioned above, J–A parameters are then coarsely identified (IDT) from these loops, creating a starting point for an optimization routine (OPT). The latter gives an initial parameter set at $t_{age} = 0$. It has been mentioned previously that the main parameter related to irreversible magnetization is the pinning factor $k$, the other J–A parameters not being directly related to this effect. Thereafter, there is no need to re-identify these parameters from scratch, as $\alpha_0$, $a_0$, $c_0$ and $M_{sat}$ are kept constant and will not be further optimized during the following time

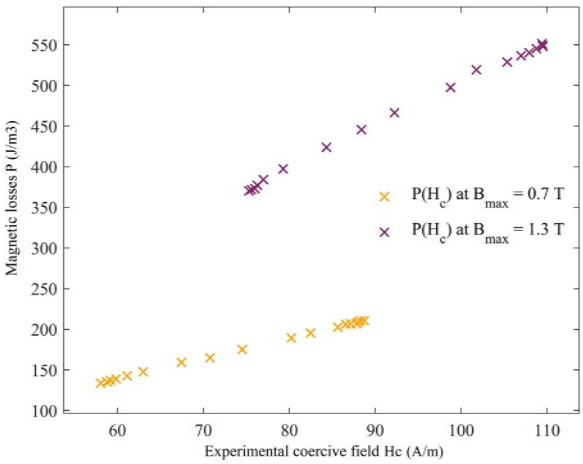


**Fig. 5.** Magnetic losses evolution with coercive field at different aging times at 200 °C and for different induction levels at $f = 5$ Hz.

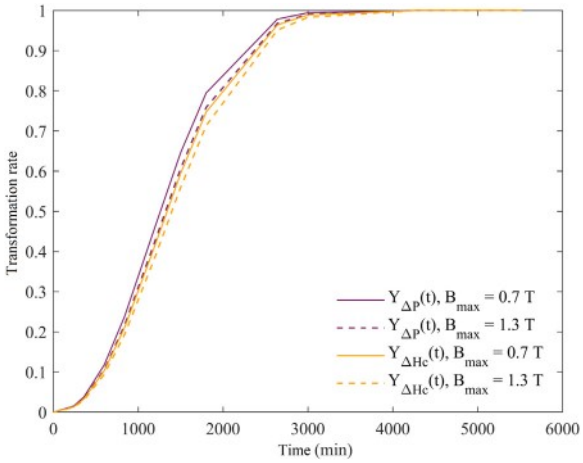


**Fig. 6.** Transformation rates of coercive field $Y_{\Delta Hc}$ and losses $Y_{\Delta P}$ measured at 200 °C, for different induction levels at 5 Hz.

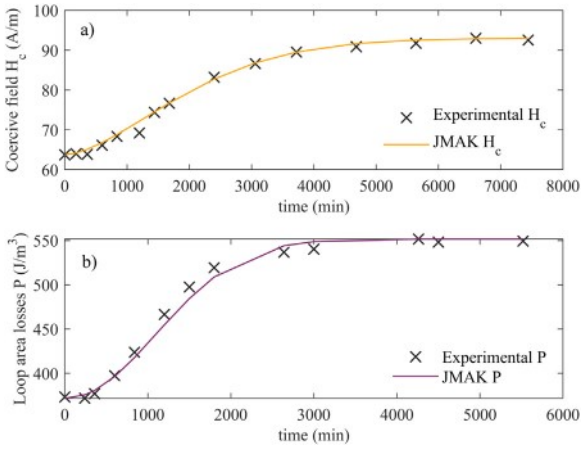


**Fig. 7.** (a) Coercive field evolution with time at 180 °C at $B_{max} = 1.3$ T, $f = 5$ Hz. (b) Hysteresis losses evolution with time at 200 °C at $B_{max} = 1.3$ T, $f = 5$ Hz.

**Table 2**
Initial optimized Jiles–Atherton parameters.

| Parameter | Value | Unit |
|---|---|---|
| $\alpha_0$ | $1.155 \times 10^{-4}$ | – |
| $a_0$ | 45.3274 | A/m |
| $c_0$ | 0.0612 | – |
| $M_{sat}$ | $1.475 \times 10^{6}$ | A/m |

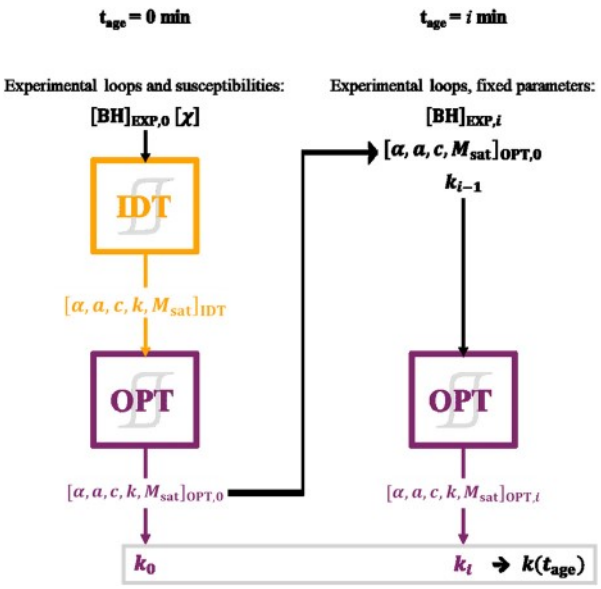


**Fig. 8.** Pinning factor extraction method.

steps $t_{age,i}$. Their fixed values are reported in Table 2. Hence, only the pinning factor $k$ will go through the next optimization steps, remaining the only aging-dependent parameters to tune.

From the aforementioned method, a set of ($t_{age,i}$, $k_i$), where $k_i$ are fitted values through the J–A approach, describing the evolution of the pinning factor with time is exposed on Fig. 9, then plotted against experimental coercive field values on Fig. 10. With $k$ being linearly related to $H_c$, which in turn shares a linear relationship with the transformation rate $Y$, the variation of the pinning factor should verify the JMAK approach (see Section 3.B.). From then on, and considering (2), it is possible to extract the $\mathcal{K}_T$ and $n$ coefficients, with the latter being kept constant. Arrhenius parameters for pinning factor description are then obtained through scatter plot linear regression and their values are listed in Table 3, to be later reused in drawing either losses or coercivity evolutions. Hence, as it can be seen on Fig. 9, in addition to following the same kinetics, pinning factor evolution with time can be quite accurately modeled, each value computed with (4) rewritten and injected in (17):

$$k(t) = k_{\min} + Y(t)\left(k_{\max} - k_{\min}\right) \tag{17}$$

The evolution of the pinning factor can therefore be expressed with the transformation rate. But to better include the temperature role, adding an Arrhenius layer to the $k$ dynamic should attain this goal. The idea behind this technique is to keep the relative difference between experimental and simulated hysteresis branches as low as possible to ensure proper fitting and a good modeling of losses and coercive field.

### 4.3. Multi-scale coupling results

At this point, it is interesting to mention that for the same material, transformation rates of other quantities can be modeled with the same Arrhenius coefficients, *e.g.*: Table 3, as Fig. 11 demonstrates. With the

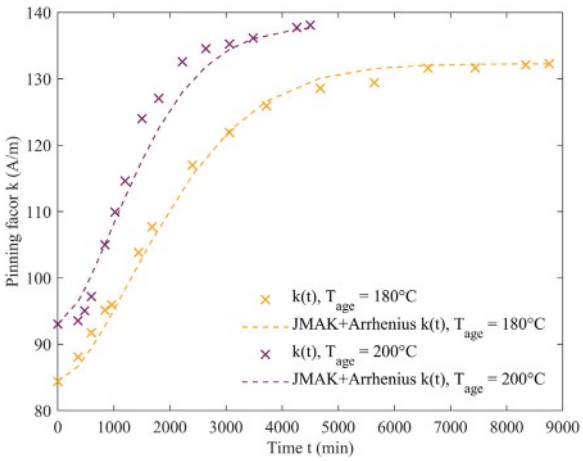


**Fig. 9.** JMAK (Arrhenius) evolution of the pinning factor with time.

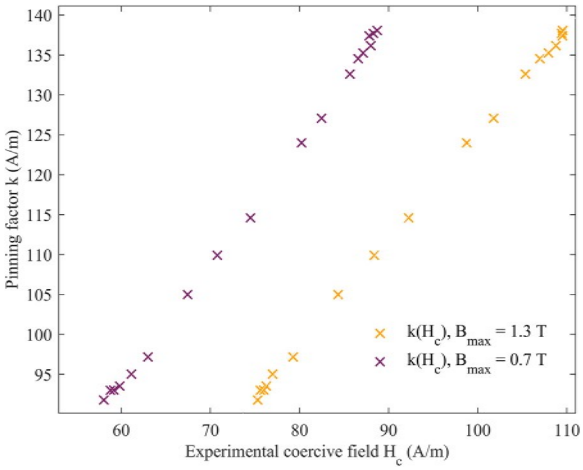


**Fig. 10.** Pinning factor in function of experimental coercive field at 200 °C.

**Table 3**
JMAK (with Arrhenius) expression coefficients.

| $T_{age}$ | $n$ | $K_T$ (J/mol) | $k_0$ ($s^{-1}$) | $Q$ (J/mol) |
|---|---|---|---|---|
| 200 °C | 2.2651 | $4.621 \times 10^{-8}$ | – | – |
| 180 °C | 1.3422 | $3.025 \times 10^{-5}$ | – | – |
| Arrhenius | 1.6205 | – | 0.4789 | 26 436 |

JMAK model applied to the evolution of the J–A pinning factor, this sections aims at replacing the expression of the latter in the J–A model with (17), resulting in coupled model. Here, the objective is to draw simulated hysteresis loops as close to their experimental counterparts as possible, with respect to loop area losses and coercive field values. From the procedure developed above, initial J–A parameters are identified and optimized on several experimental loops such as $B_{max} \in [0.7; 1.3]$ T and kept constant thereafter (see Table 2), except for the pinning factor $k$ that follows the JMAK and Arrhenius expression of (17). Experimental and simulated hysteresis loops for a maximal induction of $B_{max} = 1.3$ T are then plotted on Fig. 12, and some magnetic properties are displayed in Fig. 13.

From Fig. 12, and as Fig. 13 suggests, a rather accurate fitting of experimental loops, with respect to area losses *i.e.*, hysteresis losses and coercive field values can be expected, with an overall relative difference of less than 10%. While discrepancies in coercive field modeling are more significant, the evolution of monitored magnetic characteristics seems satisfactory. The J–A pinning factor $k(t)$ evolution, following a JMAK rule, could therefore model magnetic aging.

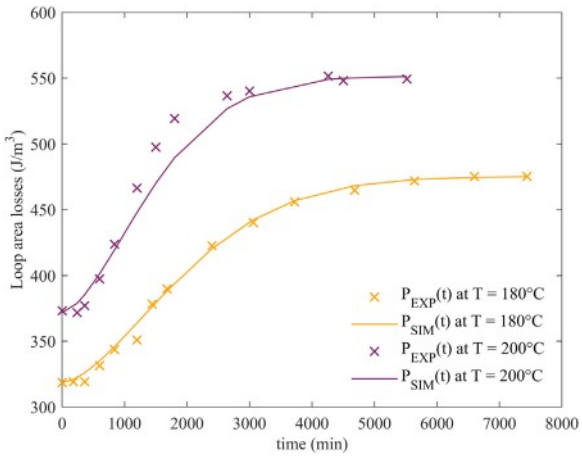


**Fig. 11.** JMAK (Arrhenius) fitting of hysteresis losses with coefficients identified on the J–A pinning factor data at $B_{max} = 1.3$ T, $f = 5$ Hz.

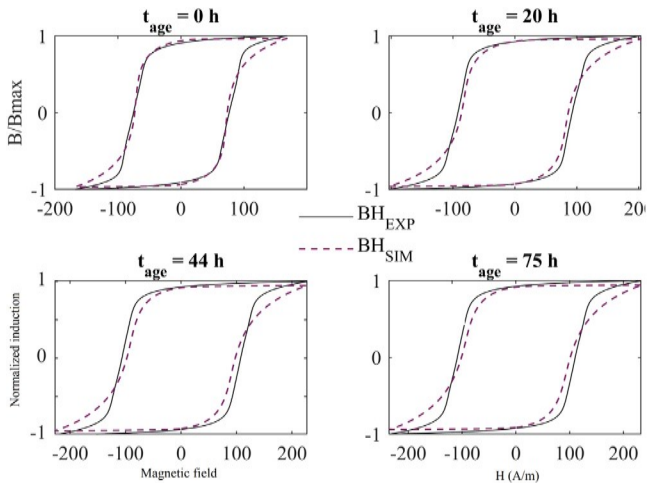


**Fig. 12.** Normalized experimental and simulated B–H loops for different aging times at $T_{age} = 200$ °C, $B_{max} = 1.3$ T, $f = 5$ Hz.

## 5. Discussion

In the following, the interest of using the J–A model instead of the standard Steinmetz model already presented in [9] will be discussed. First and foremost, the choice of model depends on the quantities of interest. If only coercive field or hysteresis losses are to be monitored, then the JMAK model alone, directly applied to $H_c$ or $P_s$ may be prioritized, as per demonstrated by [9]. However, if knowing the effects of magnetic aging on other properties is required, such as the form and width of static hysteresis loops, the presented J–A model, coupled with the JMAK expression, may be best fitted for this purpose. Moreover, the use of the J–A model allows to consider the time-evolution of the magnetic field, which in turns enables to address the dynamic effects introduced by eddy currents. In practice, these eddy currents can appear with complex temporal evolutions of the magnetic field, as it can be the case in rotating electrical machines, for example. While the proposed method builds itself on arbitrarily-chosen maximal induction amplitudes, *i.e.*, ranging from 0.7 to 1.3 T, more classical approaches to hysteresis modeling often consider B–H loops such as $B_{max} \in [0.5, 1.0, 1.5]$ T. Therefore, an extrapolation of the results presented above is performed on more *conventional* loops and drawn on Figs. 14 and 15. Hysteresis losses are reported in Table 4 to explore the technique's limits.

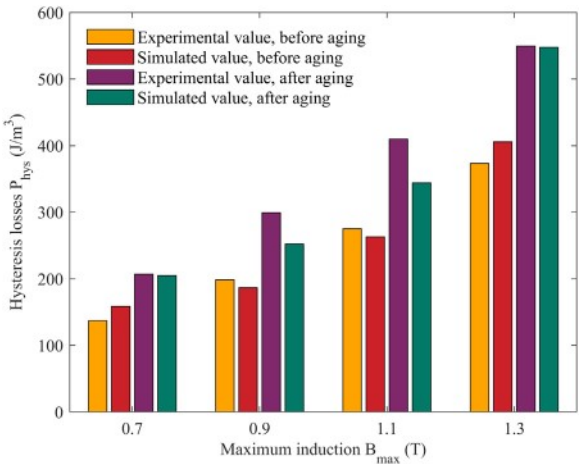


**Fig. 13.** Experimental and simulated values of hysteresis losses $T_{age} = 200$ °C.

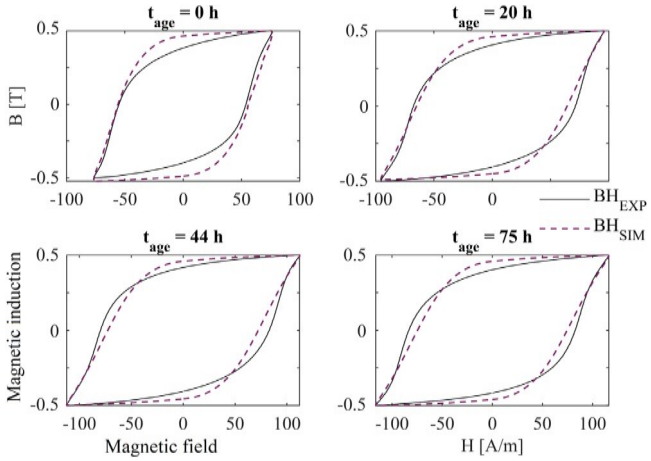


**Fig. 14.** Extrapolated experimental and simulated B–H loops at $T_{age} = 200$ °C, $B_{max} = 0.5$ T.

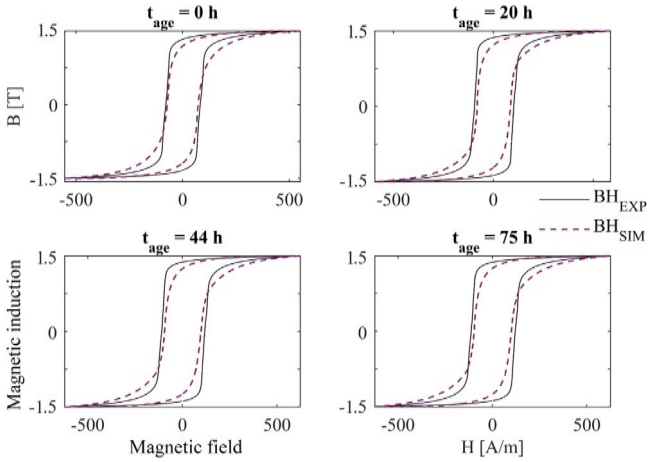


**Fig. 15.** Extrapolated experimental and simulated B–H loops at $T_{age} = 200$ °C, $B_{max} = 1.5$ T.

As both the figures and the loop areas values show, it is possible to model hysteresis loops that have not been included in the identification procedure mentioned above, with a relative error maintained around 10%. Another key point to account for is considering non-isothermal

**Table 4**
Experimental and simulated (extrapolated) values of hysteresis losses at $T_{age}$ = 200 °C.

| $t_{age}$ (h) | $P_{EXP}$ (J/m$^3$) $B$ = 0.5 T | $P_{SIM}$ (J/m$^3$) $B$ = 0.5 T | $P_{EXP}$ (J/m$^3$) $B$ = 1.5 T | $P_{SIM}$ (J/m$^3$) $B$ = 1.5 T |
|---|---|---|---|---|
| 0 | 435 | 496 | 2497 | 2491 |
| 20 | 563 | 582 | 3127 | 2774 |
| 44 | 668 | 673 | 3594 | 3289 |
| 75 | 681 | 698 | 3658 | 3379 |

aging within the 180–200 °C operating temperature range. Arrhenius-based calculations (4) open perspectives for losses prediction under complex, non-isothermal heating cycles. Last but not least, even if the results prove to align quite well with theory, the proposed model is all but predictive. Although modeling a given sample's aging from its initial state is possible, one maximal, *end of aging* value for any magnetic characteristic is still needed to perform accurate modeling of a sample batch.

## 6. Conclusion

This article shows the applicability of the JMAK approach to linearly-related magnetic quantities extracted from SST measurements of non-oriented Fe-2.3 wt% Si M600-65A soft samples. From a non-aged initial state, it is possible to identify parameters describing hysteresis behaviors, especially the J–A pinning factor $k$ that translates domain wall impingement by carbides, leading to increased coercive field and losses, *i.e.*, magnetic aging. This multi-scale coupling attempt, although rather basic, seems to accurately model magnetic aging kinetics under operating temperatures over time. To further enhance the proposed model, SST characterization will be carried out on samples of which chemical composition is known; the idea being adding layers and precision to the approach and further link material characteristics to magnetic properties and, eventually, being able to predict such a phenomenon.

## CRediT authorship contribution statement

**Fabien Dancoisne:** Writing – original draft, Validation, Methodology, Investigation, Formal analysis, Conceptualization. **Hugo Helbling:** Writing – review & editing, Resources, Formal analysis, Data curation. **Abdelkader Benabou:** Writing – review & editing, Supervision, Methodology, Investigation, Conceptualization. **Stéphane Clénet:** Writing – review & editing, Supervision, Methodology, Investigation, Conceptualization. **Myriam Dumont:** Writing – review & editing, Supervision, Methodology, Investigation, Conceptualization.

## Declaration of competing interest

The authors declare the following financial interests/personal relationships which may be considered as potential competing interests: DUMONT Myriam reports financial support was provided by French National Research Agency. If there are other authors, they declare that they have no known competing financial interests or personal relationships that could have appeared to influence the work reported in this paper.

## Acknowledgments

The author would like to thank the French National Research Agency (ANR) for its help in funding project (conferences attendance, workshops...) through the following project: MASTERMIND2 (ANR-22-CE50-0012-01).

## Data availability

Data will be made available on request.

## References

[1] L. Néel, Nouvelle théorie du champ coercitif, Physica 15 (1) (1949).
[2] L.J. Dijkstra, C. Wert, Effect of inclusions on coercive force of iron, Phys. Rev. 79 (6) (1950).
[3] S. Ray, Magnetic ageing characteristics of low silicon electrical steels, J. Magn. Magn. Mater. 28 (1982).
[4] R. Gautam, D.B. Prabhu, V. Chandrasekaran, R. Gopalan, G. Sundararajan, Influence of nanoprecipitates, solid solution and grain size on the magnetic and electrical properties of Fe–P–Si alloys, J. Magn. Magn. Mater. 493 (2020).
[5] J.R. de Oliveira-Júnior, et al., Kinetics of magnetic ageing of 2% Si non-oriented grain electrical steel, Mater. Res. 21 (1) (2018).
[6] A.A. de Almeida, F.J.G. Landgraf, Magnetic aging, anomalous and hysteresis losses, Mater. Res. 22 (3) (2019).
[7] G.M.R. Negri, N. Sadowski, N.J. Batistela, J.V. Leite, J.P.A. Bastos, Magnetic aging effect losses on electrical steels, IEEE Trans. Magn. 52 (5) (2016).
[8] M.F. de Campos, et al., Consequences of magnetic aging for iron losses in electrical steels, J. Magn. Magn. Mater. 304 (2) (2006).
[9] M. Jamil, et al., Application of the JMAK precipitation law in iron loss modelling to account for magnetic ageing effect, J. Magn. Magn. Mater. 547 (2022).
[10] H. Helbling, M. Toto-Jamil, M. Dumont, A. Benabou, S. Clénet, Temperature-dependent modelling of magnetic ageing of FeSi electrical steels, J. Magn. Magn. Mater. 564 (2022).
[11] J.W. Christian, The Theory of Transformations in Metals and Alloys (Part I), 1965.
[12] M. Perez, M. Dumont, D. Acevedo-Reyes, Implementation of classical nucleation and growth theories for precipitation, Acta Mater. (2008).
[13] W.A. Johnson, R.F. Mehl, Reaction kinetics in processes of nucleation and growth, Trans. Am. Inst. Min. Met. Eng. 135 (1939).
[14] M. Avrami, Kinetics of phase change, I general theory, J. Chem. Phys. 7 (12) (1939).
[15] A.N. Kolmogorov, On the statistical theory of the crystallization of metals, Bull. Acad. Sci. USSR Math. Ser. 1 (3) (1937).
[16] M. Fanfoni, M. Tomellini, The Johnson–Mehl–Avrami–Kolmogorov Model: A Brief Review, 1998.
[17] D.A. Porter, K.E. Easterling, Phase Transformation in Metals and Alloys, second ed., Chapman & Hall, 1992.
[18] D.C. Jiles, D.L. Atherton, Theory of ferromagnetic hysteresis, J. Appl. Phys. (1984).
[19] D.C. Jiles, J.B. Thoelke, M.K. Devine, Numerical determination of hysteresis parameters the modeling of magnetic properties using the theory of ferromagnetic hysteresis, IEEE Trans. Magn. 28 (I) (1992).
[20] P. Weiss, L'hypothèse du champ moléculaire et la propriété ferromagnétique, J. Phys. Theor. Appl. 6 (1907) 4ème série.
[21] D.C. Jiles, J.B. Thoelke, Theory of ferromagnetic hysteresis: Determination of model parameters from experimental hysteresis loops, IEEE Trans. Magn. 25 (1989).
[22] S. Clénet, et al., Determination of losses' local distribution for transformer optimal designing, COMPEL 20 (2001).
[23] A. Benabou, Caractérisation et modélisation des matériaux magnétiques pour les dispositifs de conversion électromagnétique de l'énergie, mémoire d'HDR, 2015.
[24] F. Dancoisne, M. Dumont, S. Clénet, A. Benabou, Modélisation du vieillissement magnétique des aciers électriques Fe–3%Si, in: Symposium de Génie Électrique, 2023.